Degradation of oxygen reduction reaction kinetics in porous La$_{0.6}$Sr$_{0.4}$Co$_{0.2}$Fe$_{0.8}$O$_{3-\delta}$ cathodes due to aging-induced changes in surface chemistry

Laura C. Baqué [a, *], Analía L. Soldati [a], Erico Teixeira-Neto [b], Horacio E. Troiani [a], Anja Schreiber [c], Adriana C. Serquis [a]

[a] CNEA, CONICET, Centro Atómico Bariloche, Av. Bustillo 9500, R8402AGP, S. C. de Bariloche, Argentina
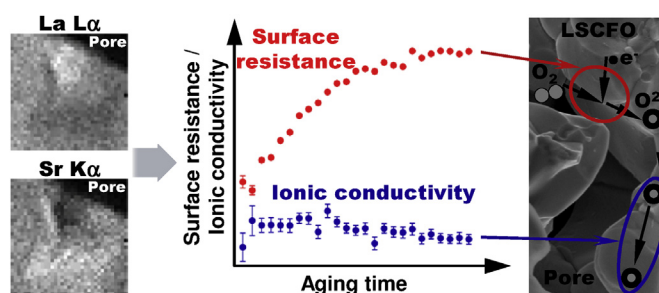[b] Brazilian Nanotechnology National Laboratory, Brazilian Center for Research in Energy and Materials, Rua Giuseppe Máximo Scolfaro, 10.000, Campinas, Brazil
[c] Helmholtz-Zentrum Potsdam, Deutsches GeoForschungsZentrum GFZ, Sektion 4.2, Geomechanik und Rheologie, Telegrafenberg, C 155, D-14473, Potsdam, Germany

HIGHLIGHTS

- Surface La- and Sr-enrichment induced by aging LSCFO cathodes at 800 °C for 50 h.
- Cation redistribution can extend up to ~400 nm depth under the LSCFO surface.
- Surface chemical changes detected by high resolution STEM/EDS maps at cathode pores.
- Oxygen exchange at LSCFO/gas interface hampered by surface chemistry modification.
- Oxygen ion conductivity remains constant upon aging according to impedance analysis.

GRAPHICAL ABSTRACT

ABSTRACT

The modification of surface composition after long-term operation is one of the most reported degradation mechanisms of (La,Sr)(Co,Fe)O$_{3-\delta}$ (LSCFO) cathodes for Solid Oxide Fuel Cells (SOFCs). Nevertheless, its effect on the oxygen reduction reaction kinetics of porous LSCFO cathodes has not been yet reliably established. In this work, La- and Sr-enrichment at the LSCFO surface of porous cathodes has been induced after 50 h aging at 800 °C under air. Such cation redistribution can extend up to ~400 nm depth under the LSCFO surface as detected by high resolution Scanning Transmission Electron Microscopy-Energy Dispersive Spectroscopy maps acquired inside the cathode pores. The observed surface chemical changes hamper the oxygen surface exchange reaction at the LSCFO/gas interface. Accordingly, a suitable Electrochemical Impedance Spectroscopy analysis revealed that the oxygen ion conductivity remains practically unaltered during the aging treatment while the oxygen surface exchange resistance increases up to 1.8 times. As a result, the cathode impedance response deteriorates within the 10–0.1 Hz frequency range during the aging treatment, resulting in a total cathode area

* Corresponding author. CAB, Av. Bustillo 9500, R8402AGP, S. C. de Bariloche, RN, Argentina.
E-mail address: baquel@cab.cnea.gov.ar (L.C. Baqué).

specific resistance increase of 150%. The methodology adopted has demonstrated to be very valuable for studying the degradation of SOFC cathodes produced by the modification of surface composition.

1. Introduction

Solid Oxide Fuel Cells (SOFCs) are ceramic devices used to convert chemical energy into electricity and heat [1,2]. The operation of these devices involves the oxygen reduction at the cathode, the oxygen ion conduction through the electrolyte, and the oxidation of the fuel (e.g. hydrogen, methane, carbon monoxide) at the anode. SOFC efficiency and durability is mainly determined by the area specific resistance (ASR) and degradation of the cathode, the electrolyte and the anode. Since the cathode is typically the component with the highest ASR [3], it is very important to limit its degradation.

$(La,Sr)(Co,Fe)O_{3-\delta}$ (LSCFO) is one of the most used mixed ionic-electronic conductors for SOFC cathodes [2]. The degradation of the electrochemical response in these cathodes is usually ascribed in the literature to the modification of surface composition, mostly by Sr segregation [4–6]. This phenomenon is generally detected by using techniques with low lateral resolution as X-ray Photoelectron Spectroscopy (XPS) [7–11] or Scanning Electron Microscopy-Energy Dispersive Spectroscopy (SEM-EDS) [12–14] or by using indirect techniques such as the detection of water-soluble species by Inductively Coupled Plasma (ICP) Spectrometry [7,15–17]. No appreciable microstructural changes, as the formation of precipitates at the LSCFO surface, are normally observed in porous cathodes [7–9]. Consequently, the investigation of such degradation mechanism turns out to be challenging. Independently, several authors have reported the observation of Sr-rich and/or Co-rich precipitates in dense LSCFO pellets sintered at high temperature (i.e. $\geq$ 1250 °C) [12–14,18] or in dense $La_{1-x}Sr_xCoO_{3-\delta}$ thin films prepared by Pulse Laser Deposition (PLD) [10,11]. This suggests that surface compositional changes induced by aging are more likely to occur in dense samples than in porous ones. Nevertheless, it is not clear to what extent the results obtained with dense samples can be extrapolated to porous cathodes used in practical SOFCs. Therefore, it is necessary to investigate LSCFO cathodes under conditions which maximize the occurrence of surface chemistry degradation without losing the porous structure of practical cathodes.

In this work, we have investigated the degradation of $La_{0.6}Sr_{0.4}Co_{0.2}Fe_{0.8}O_{3-\delta}$ cathodes induced by aging at 800 °C for 50 h in ambient air. The studied cathodes have an intermediate microstructure between that of a dense pellet and that of a porous film since they are indeed porous but are mainly composed of particles within the micrometric range (as the dense pellets). This particular microstructure was chosen because our preliminary results [19] suggest that it facilitates the occurrence of noticeable surface microstructural and compositional changes under the aging conditions mentioned above. The evolution of the cathode electrochemical properties was continuously monitored by Electrochemical Impedance Spectroscopy (EIS) during the aging treatment while the cation distribution was investigated by high resolution Scanning Transmission Electron Microscopy and Energy Dispersive Spectroscopy (STEM-EDS) before and after the aging treatment.

2. Experimental section

2.1. Symmetrical cells

Commercial $Ce_{0.9}Gd_{0.1}O_{2-\delta}$ (CGO) electrolyte powders (Fuel-cellmaterials, USA) were uniaxially pressed and sintered in air at 1350 °C for 12 h for obtaining two dense substrates with 9.75 mm diameter and 1 mm thickness. Separately, $La_{0.6}Sr_{0.4}Co_{0.2}Fe_{0.8}O_{3-\delta}$ (LSCFO) cathode powders were prepared by solid state reaction. Stoichiometric amounts of $SrCO_3$, La_2O_3, Co_3O_4 and Fe_2O_3 were ball milled and sintered in air at 1000 °C for 5 h. An ink was prepared by mixing the LSCFO powders with isopropyl alcohol, alpha-terpineol, polyvinyl butyral (PVB) and polyvinyl pyrridone (PVP) in a weight ratio of 70:20:9:0.65:0.35. The LSCFO-based ink was deposited on both sides of the two CGO substrates by the spin coating technique. Cathode layers completely covered the electrolyte having a geometric area of 0.75 cm^2 each. LSCFO/CGO/LSCFO symmetrical cells were sintered in air at 1250 °C for 12 h. The obtained LSCFO cathodes were 8.5 ± 2 μm thick with grain sizes within the 40 nm–3.8 μm range and a volume median diameter [20] of 1.68 μm as determined by analyzing SEM images with the software ImageJ [21].

2.2. Cell characterization and aging treatment

One of the cells was also aged at 800 °C in air for 50 h and characterized by EIS, TEM and STEM-EDS. The other non-aged cell was studied only by TEM, and STEM-EDS as reference.

2.2.1. Microstructural characterization

The microstructure of the non-aged and the aged LSCFO/CGO/LSCFO were previously characterized by SEM and reported elsewhere [19]. Additionally, representative zones for TEM lamellae extraction were precisely selected in each sample by using a W-filament SEM (Philips 515) and a FEG-SEM (FEI Nova NanoSEM 230). Thin lamellae of ~15 × 8 × 0.1 μm^3 were extracted from the cathode/electrolyte interface by the Focused Ion Beam (FIB)/Lift-out [22] technique and deposited on a holey carbon-film supported by a copper-grid. This procedure was carried out in a FEI FIB-200 system with a Ga ion source and an acceleration voltage of 30 kV. Pt was applied on the cathode surface as a protection layer. TEM images were acquired with a Philips CM 200 UT microscope operated at 200 kV. The distribution of metal atoms within the cathodes was investigated by the acquisition of compositional maps using a JEOL-JEM 2100F microscope available at the Nanotechnology National Laboratory (LNNano) (CNPEM, Campinas, SP). The X-ray Energy Dispersive (XED)-Spectrum Imaging technique was employed with a Digital Micrograph 1.8 system (Gatan, Inc.) controlling a Thermo-Noran XEDS. The spectrum images (SI) were acquired with a dwell time of 0.5 s/pixel using the drift correction facility at every 100 s. XED spectra were acquired in the 0–20 keV energy range at each pixel. Electron probe sizes of ca. 1.5 nm were obtained operating the JEM 2100F instrument in the STEM mode, allowing enough current density at each sample point for the acquisition of statistically significant X-ray counts for the investigated elements.
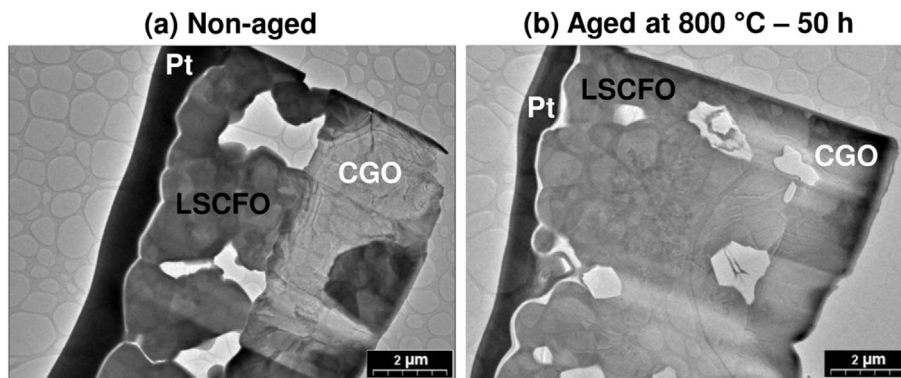
(a) Non-aged

(b) Aged at 800 °C – 50 h

Fig. 1. TEM images of the LSCFO/CGO lamellae extracted from (a) the non-aged cell and (b) the cell aged at 800 °C in air for 50 h. Pt was deposited as a protective layer.

2.2.2. Electrochemical characterization

The electrochemical response evolution of the aged cell was monitored by EIS during aging treatment at 800 °C under 100 ml/min ambient air flow. Impedance spectra were recorded every 2 h with a total measuring time of 16 min per spectrum. EIS measurements were performed by applying a 50 mV root mean square AC signal between 3×10^4 and 1×10^{-2} Hz with a potentiostat/impedance analyzer Autolab (Eco Chemie BV). Pt grids, mechanically pressed onto the cathode, were used as current collectors. The setup and the electrolyte resistances were subtracted
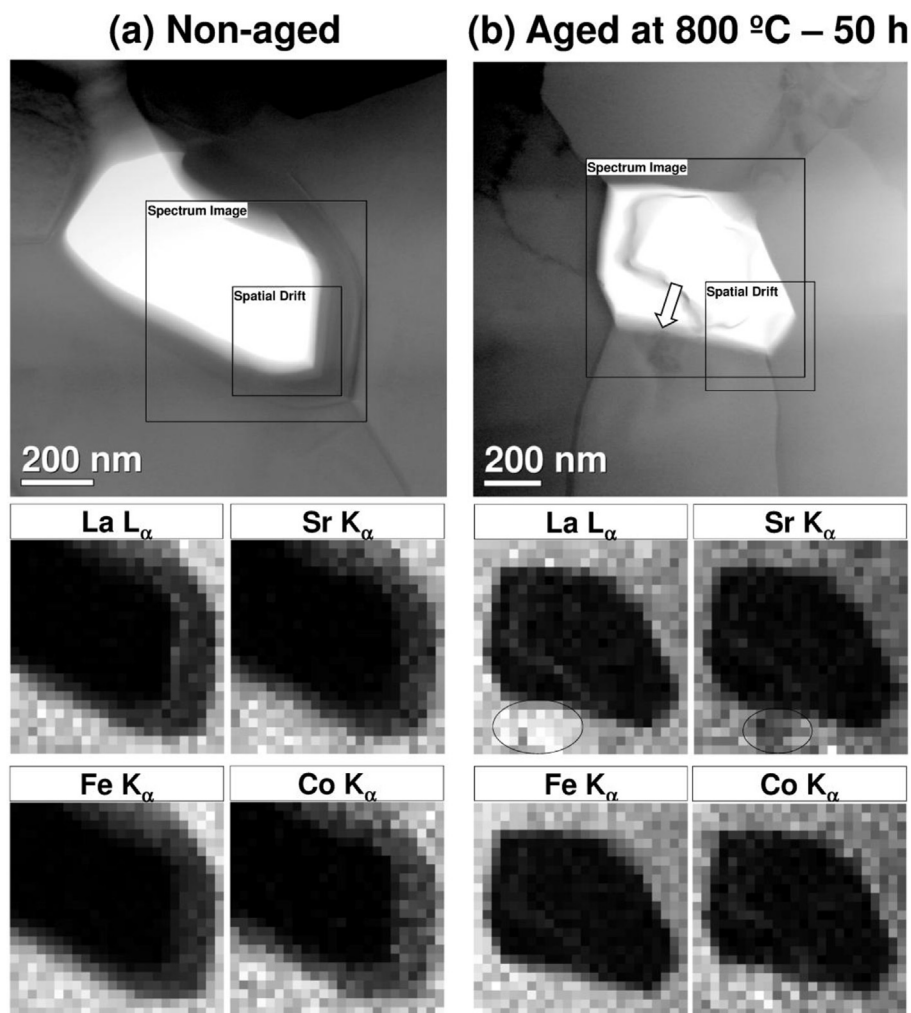
(a) Non-aged

(b) Aged at 800 °C – 50 h

Fig. 2. STEM images (top) and compositional EDS maps (bottom) around a pore of (a) the non-aged cell and (b) the cell aged at 800 °C in air for 50 h. The zone where the compositional map (spectrum image) was acquired along with the zone used for drift correction (spatial drift) are indicated by the black squares in the STEM image. The white arrow in (b) points out a wrinkle at the LSCFO surface. The black circles of the La L_α and Sr K_α element maps in (b) indicate the zones where the concentration of these elements is uneven. Pixel size of compositional maps is 25 nm in (a) and 32 nm in (b).

from all the spectra, which were then divided by 2, normalized by the cathode geometric area, and fitted with the software ZView [23]. The reported error of the fitted parameters represents the range of values which produces similar goodness of fit.

3. Results

3.1. Microstructural characterization

Fig. 1a and b show cross-section TEM images of the non-aged and the aged cells. The LSCFO/CGO interface of the aged sample looks sharp, indicating that no cathode delamination has occurred even after the aging treatment. In addition, no measurable chemical reaction [24–26] between the cathode and the electrolyte were detected.

STEM images with higher magnification were acquired around the pores of the non-aged and the aged cathodes (Fig. 2). A region with a distinctive contrast can be distinguished at the pore bottom in the aged cathode (indicated with a white arrow in Fig. 2b). The surface of this region forms a small bump or wrinkle comparable in size to those previously detected by SEM [19]. EDS element maps were acquired in order to investigate if such degradation phenomenon is also related with changes in the composition. The distribution of La, Sr, Fe and Co is homogeneous in the non-aged cathode (Fig. 2a) while only Co and Fe are uniformly distributed in the aged cathode (Fig. 2b). In contrast, La is concentrated and Sr is depleted in the regions marked with circles in Fig. 2b indicating that the distribution of these elements is uneven in the aged cathode. EDS point spectra and compositional maps acquired with higher spatial resolution allow distinguishing zones with different cation concentrations in the aged sample (see Fig. 3). The zone with the highest proportional concentration of La and the lowest proportional concentration of Sr (Zone 1) is at the pore surface and has an extension of 125 nm × 135 nm approximately. Zone 2, located next to zone 1, has similar La and Sr concentration that zones 3 and 4 which extend towards the bulk. Zones 1 and 2 are surrounded by zone 5 which is the richest in Sr and the poorest in La, has a width of 50–80 nm, and extends up to ~400 nm under the surface. Co and Fe concentration is similar in all the measured EDS spectra.

3.2. Electrochemical characterization

The impedance response evolution of LSCFO/CGO/LSCFO cell with aging time is shown in Fig. 4. The total ASR significantly increases during the first hours of the aging treatment and then it tends to stabilize (Fig. 4a). The aging treatment affects the EIS
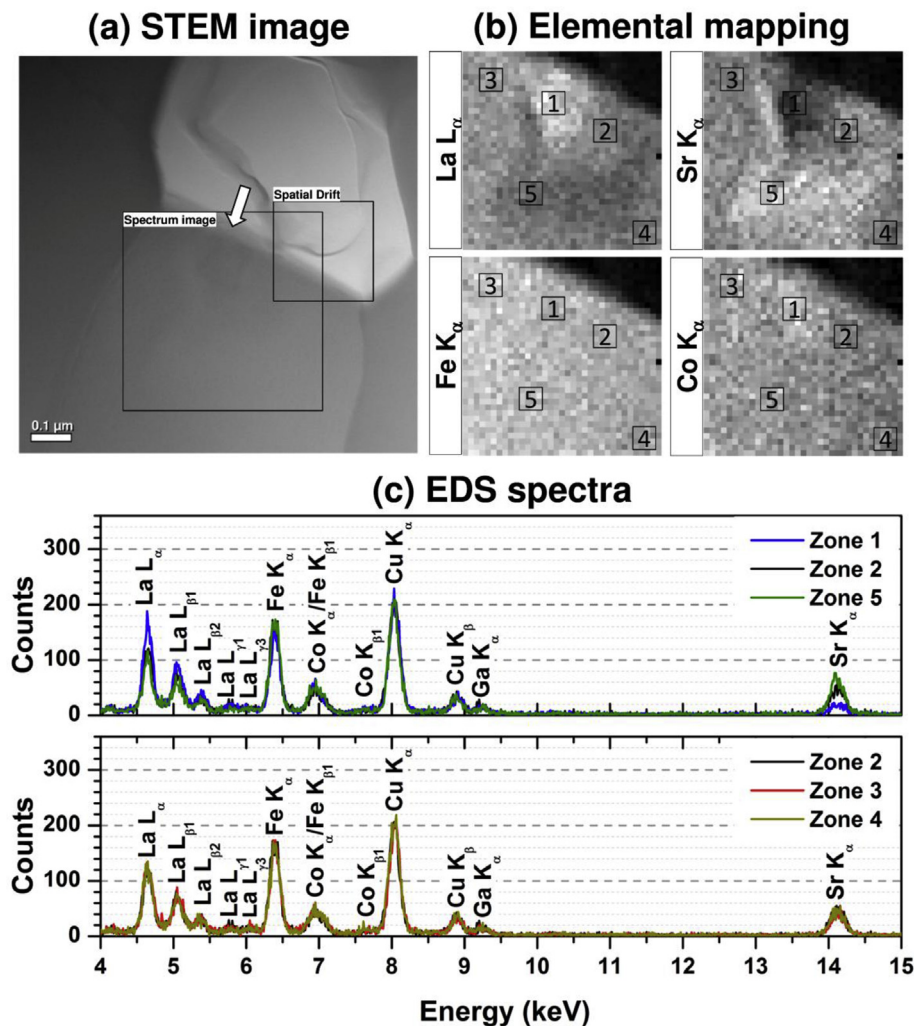

Fig. 3. Detailed EDS compositional analysis of the aged cathode in the same area of Fig. 2b. (a) STEM image. The white arrow indicates a wrinkle at the LSCFO surface. The zone labeled as spectrum image indicates where the compositional map was acquired while the zone named spatial drift indicates the zone used for drift correction. (b) Element maps were acquired using a pixel size of 15 nm. (c) Normalized point EDS spectra acquired in the zones indicated in (b).
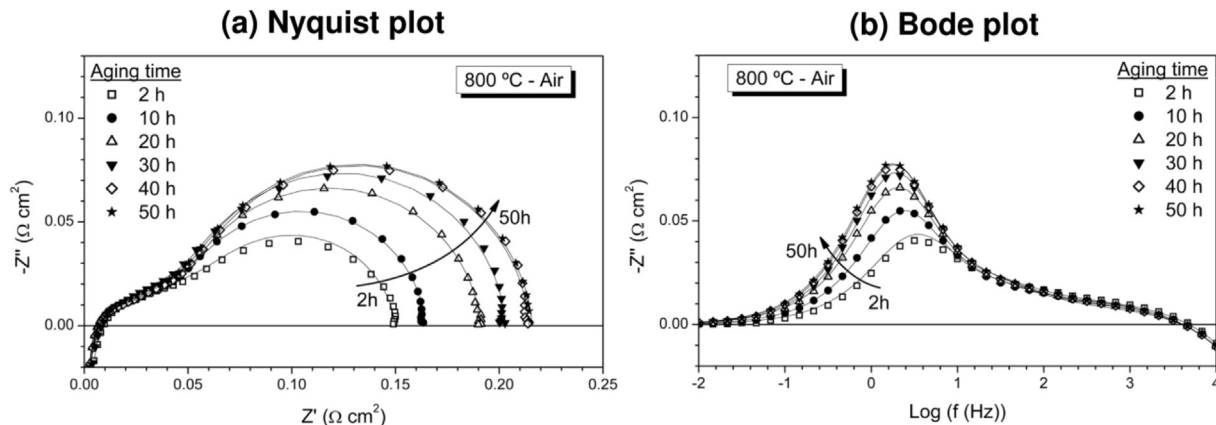
(a) Nyquist plot

(b) Bode plot

Fig. 4. (a) Nyquist and (b) bode plots of the impedance response of a LSCFO/CGO/LSCFO cell as a function of time during aging at 800 °C in air. Points represent the raw data and lines represent the fitting results using the equivalent circuit in Fig. 5.

spectra only within the 10−0.1 Hz frequency range (Fig. 4b). All measured EIS spectra were fitted by using the equivalent circuit shown in Fig. 5. This equivalent circuit was selected based on the shape of the EIS spectra, on previous results reported in literature [27−32], and on the physical and electrochemical phenomena occurring during the impedance measurements. The element L_c denotes the inductance of the connector cables, the sub-circuit composed of the resistance R_{HF} in parallel with the constant phase element CPE_{HF} can be ascribed to the cathode/electrolyte interface [27−29], and the impedance Z_{chem} represents the oxygen reduction reaction at the mixed ionic-electronic conducting cathode. R_{HF} values remain constant during all the aging treatment (Fig. 6). Instead, R_{Chem} (i.e. the real part of Z_{Chem}) values increase up to 1.5 times in the first 26 h of the aging treatment becoming more stable for longer aging times.

The impedance Z_{Chem} can be derived from the well-known Adler-Lane-Steele model [30−32] (see the Supplementary data) leading to the following expression [33−35]:

$$Z_{Chem} = \sqrt{r_{bulk}r_{surface}}\sqrt{\frac{1}{1+(j\omega)^n r_{surface}q_{surface}}}$$
$$\coth\left(L\sqrt{\frac{r_{bulk}}{r_{surface}}}\sqrt{1+(j\omega)^n r_{surface}q_{surface}}\right) \quad (1)$$

where r_{bulk} is a distributed resistance related to the oxygen ion diffusion through the bulk, $r_{surface}$ and $q_{surface}$ are a distributed resistance and a distributed capacitance related to the oxygen surface exchange reaction, L is the cathode thickness, and n is a coefficient accounting the non-ideal response of practical electrodes with rough surfaces [36−38]. r_{bulk}, $r_{surface}$, $q_{surface}$ and n are the fitted parameters while L is fixed. The n values fitted range from 0.92 to 0.96 for all the spectra. In addition, the effective ionic conductivity of the cathode ($\sigma_{cathode}$) can be estimated as $1/r_{bulk}$. Fig. 7 shows the evolution of $\sigma_{cathode}$ and $r_{surface}$ with aging time.
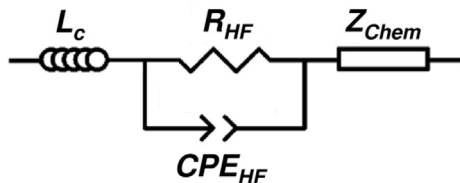
$\sigma_{cathode}$ values remains practically constant during the aging treatment while $r_{surface}$ values increase up to 1.7 times in the first 26 h of aging and then tends to stabilize in a $r_{surface}$ value 1.8 times higher than the initial one.

4. Discussion

The only cathode degradation mechanism detected within the limits of this study is the modification of the cation concentration at the LSCFO surface. While most research efforts focuses in studying only the top surface of the samples, the use of the high resolution STEM-EDS technique has allowed us demonstrating that such chemical phenomena can also occur at the LSCFO surface inside the pores. The formation of Sr- and/or Co-rich particles on the top surface of dense LSCFO samples has been reported by several authors [10−14,18] while only surface Sr-enrichment without microstructural changes is usually observed in aged porous LSCFO cathodes [7−9]. Instead, our STEM-EDS results indicate the presence of both Sr- and La-rich regions at the aged LSCFO surface similarly to the findings of Bucher et al. [39]. The La-rich region is also Sr-depleted while the Sr-rich region is La-depleted. This later phenomenon is comparable to that reported by Druce et al. [40]. The fact that both La and Sr cations redistribute is in agreement with the similar diffusion coefficients reported for both cations in La$_{0.6}$Sr$_{0.4}$CoO$_{3-\delta}$ films [41]. In addition, our findings reveals that the
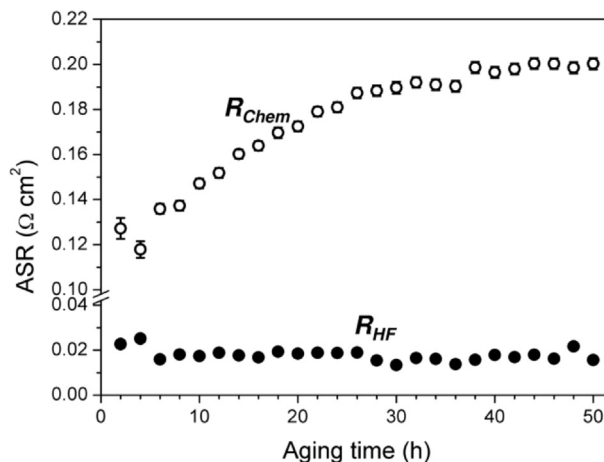

Fig. 5. Equivalent circuit used for fitting the EIS spectra in the whole frequency range.

Fig. 6. Evolution of R_{HF} and R_{Chem} values with aging time.

(a) Cathode ionic conductivity
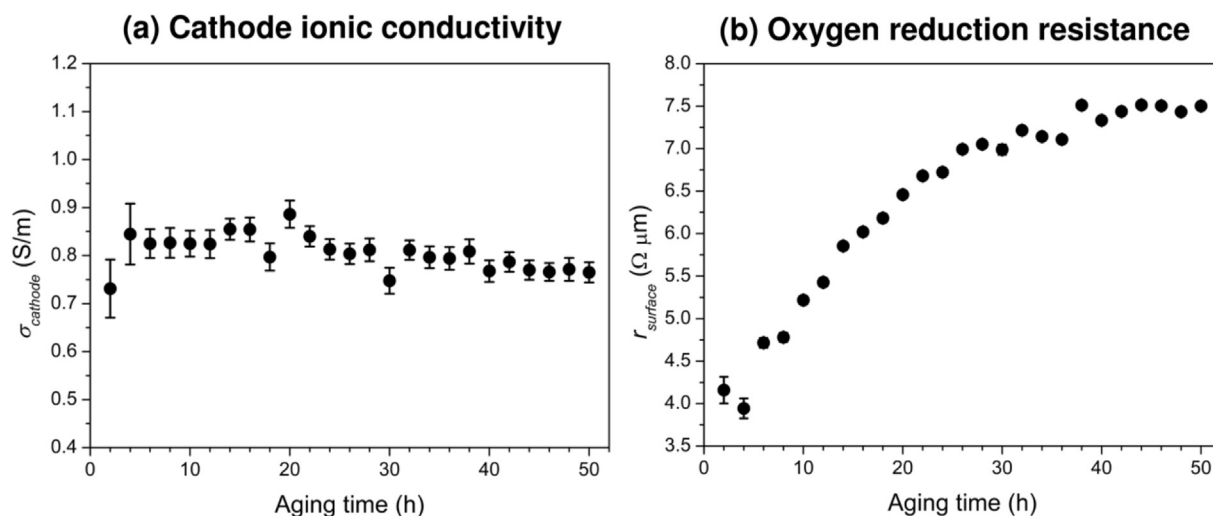
(b) Oxygen reduction resistance

Fig. 7. Evolution of $\sigma_{cathode}$ and $r_{surface}$ with aging time. The scale of each graph was adjusted so that the error bars representing equal relative errors have the same length in both graphs.

cation enriched regions can be as narrow as 50—120 nm but extending up to ~400 nm depth which is larger than the 30—75 nm depth previously reported in the literature determined by techniques with low lateral resolution as XPS [9,39]. All the above indicates that modification of cathode surface after aging is a complex three-dimensional phenomenon that requires the use of techniques with high lateral resolution (i.e. at least few tens of nm) for its appropriate characterization.

Our results also show that the high frequency contribution of the EIS spectra (i.e. $R_{HF}//CPE_{HF}$) doesn't change with aging time, which is consistent with the fact that no deterioration of the cathode/electrolyte interface was detected. EIS spectra are affected only in the low frequency range during aging treatment agreeing with the observations reported by other authors for LSCFO cathodes exhibiting changes in the surface chemistry induced by different treatments [7—9,17,42]. Our EIS analysis based on the ALS model allowed separating the contributions of the oxygen ion diffusion and the oxygen surface exchange to the cathode ASR increase. Similarly, Wang et al. [7] have used the ALS model for studying the evolution of the oxygen surface exchange rate and the oxygen diffusion coefficient in porous LSCFO cathodes after aging at 800 °C for 800 h in ambient air. They found a decrease of about 50% in both parameters even though the only chemical and microstructural degradation mechanism detected was Sr-enrichment at the surface. The authors attributed the unexpected change in the oxygen diffusion coefficient either to a limitation of the used approach for separating each contribution or to a decrease in the oxygen ionic conductivity produced by the Sr-depleted sub-surface. In contrast, an increase of up to 180% in the oxygen surface exchange resistance without a significant change in the oxygen ionic conductivity was detected by our EIS analysis. This is consistent with the observed compositional changes since La- and Sr-enrichment at the LSCFO surface has been demonstrated to decrease its oxygen surface exchange coefficient without affecting the bulk conductivity [39]. The decrease of the oxygen surface exchange coefficient, reflected by the increase in $r_{surface}$ values, therefore causes the cathode ASR increase which would deteriorate the fuel cell performance with aging time [3].

5. Conclusions

Cation redistribution at the LSCFO surface has been induced by

aging porous cathodes at 800 °C in air for 50 h. Sr-enriched/La-depleted and La-enriched/Sr-depleted regions (extending up to ~400 nm underneath the surface) were detected by high resolution STEM-EDS mapping at the LSCFO/gas interface inside the cathode pores. It demonstrates that this degradation mechanism is not only limited to the top cathode surface as usually reported in the literature. An adequate EIS analysis, derived from the Adler-Lane-Steele model, allowed investigating separately the evolution of the oxygen ion conductivity and the oxygen surface exchange resistance. No significant variations in the oxygen ion conductivity were observed during the aging treatment. Conversely, the oxygen surface exchange resistance increases up to 1.8 times upon aging indicating that the oxygen surface exchange reaction is hindered by the chemical changes observed at the LSCFO surface. As a result, EIS spectra vary significantly during the aging treatment within the 10—0.1 Hz frequency range and the cathode ASR increases up to 150%. Based on the results above, the adopted methodology was successful in reliably determining the effects of surface chemistry modification on the impedance response of porous LSCFO cathodes. Therefore, it can be surely applied for studying similar degradation mechanisms in other cathode compositions and establishing a correlation between the cation surface characteristics and the electrochemical behavior.

Appendix A. Supplementary data

Supplementary data related to this article can be found at http://dx.doi.org/10.1016/j.jpowsour.2016.10.090.

References

[1] B.C.H. Steele, A. Heinzel, Materials for fuel-cell technologies, Nature 414 (2001) 345—352.
[2] N. Mahato, A. Banerjee, A. Gupta, S. Omar, K. Balani, Progress in material

selection for solid oxide fuel cell technology: a review, Prog. Mater. Sci. 72 (2015) 141–337.

[3] E. Ivers-Tiffée, A. Weber, D. Herbstritt, Materials and technologies for SOFC-components, J. Eur. Ceram. Soc. 21 (2001) 1805–1811.

[4] J. Druce, H. Téllez, J. Hyodo, Surface segregation and poisoning in materials for low-temperature SOFCs, MRS Bull. 39 (2014) 810–815.

[5] R. Knibbe, A. Hauch, J. Hjelm, S.D. Ebbesen, M. Mogensen, Durability of solid oxide fuel cells, Green 1 (2011) 141–169.

[6] H. Yokokawa, H. Tu, B. Iwanschitz, A. Mai, Fundamental mechanisms limiting solid oxide fuel cell durability, J. Power Sources 182 (2008) 400–412.

[7] H. Wang, K.J. Yakal-Kremski, T. Yeh, G.M. Rupp, A. Limbeck, J. Fleig, S.A. Barnett, Mechanisms of performance degradation of (La,Sr)(Co,Fe)O$_{3-\delta}$ solid oxide fuel cell cathodes, J. Electrochem. Soc. 163 (2016) F581–F585.

[8] Z. Pan, Q. Liu, L. Zhang, X. Zhang, S.H. Chan, Effect of Sr surface segregation of La$_{0.6}$Sr$_{0.4}$Co$_{0.2}$Fe$_{0.8}$O$_3$ electrode on its electrochemical performance in SOC, J. Electrochem. Soc. 162 (2015) F1316–F1323.

[9] S.P. Simner, M.D. Anderson, M.H. Engelhard, J.W. Stevenson, Degradation mechanisms of La-Sr-Co-Fe-O$_3$ SOFC cathodes, Electrochem. Solid State Lett. 9 (2006) A478–A481.

[10] N. Tsvetkov, Q. Lu, L. Sun, E.J. Crumlin, B. Yildiz, Improved chemical and electrochemical stability of perovskite oxides with less reducible cations at the surface, Nat. Mater. 15 (2016) 1010–1016.

[11] Z. Cai, M. Kubicek, J. Fleig, B. Yildiz, Chemical heterogeneities on La$_{0.6}$Sr$_{0.4}$CoO$_{3-\delta}$ thin films-correlations to cathode surface activity and stability, Chem. Mater. 24 (2012) 116–1127.

[12] M.A. Niania, R. Podor, S.J. Skinner, J.A. Kilner, In-situ surface analysis of SOFC cathode degradation using high temperature enviromental scanning electron microscopy, ECS Trans. 68 (2015) 665–670.

[13] L. Zhao, J. Drennan, C. Kong, S. Amarasinghe, S.P. Jiang, Insight into surface segregation and chromium deposition on La$_{0.6}$Sr$_{0.4}$Co$_{0.2}$Fe$_{0.8}$O$_{3-\delta}$ cathodes of solid oxide fuel cells, J. Mater. Chem. A 2 (2014) 11114–11123.

[14] W. Araki, T. Yamaguchi, Y. Arai, J. Malzbender, Strontium surface segregation in La$_{0.58}$Sr$_{0.4}$Co$_{0.2}$Fe$_{0.8}$O$_{3-\delta}$ annealed under compression, Solid State Ion. 268 (2014) 1–6.

[15] G.M. Rupp, H. Téllez, J. Druce, A. Limbeck, T. Ishihara, J. Kilner, J. Fleig, Surface chemistry of La$_{0.6}$Sr$_{0.4}$CoO$_{3-\delta}$ thin films and its impact on the oxygen surface exchange resistance, J. Mater. Chem. A 3 (2015) 22759–22769.

[16] G.M. Rupp, A. Limbeck, M. Kubicek, A. Penn, M. Stöger-Pollach, G. Friedbacher, J. Fleig, Correlating surface cation composition and thin film microstructure with the electrochemical performance of lanthanum strontium cobaltite (LSC) electrodes, J. Mater. Chem. A 2 (2014) 7099–7108.

[17] M. Kubicek, A. Limbeck, T. Frömling, H. Hutter, J. Fleig, Relationship between cation segregation and the electrochemical oxygen reduction kinetics of La$_{0.6}$Sr$_{0.4}$CoO$_{3-\delta}$ thin film electrodes, J. Electrochem. Soc. 158 (2011) B727–B734.

[18] D. Oh, D. Gostovic, E.D. Wachsman, Mechanism of La$_{0.6}$Sr$_{0.4}$Co$_{0.2}$Fe$_{0.8}$O$_{3-\delta}$ cathode degradation, J. Mater. Res. 27 (2012) 1992–1999.

[19] L. Baqué, A. Soldati, H. Troiani, A. Serquis, Effect of cation demixing on the electrochemical performance of LSCFO cathodes for SOFCs, ECS Trans. 64 (2014) 11–16.

[20] R.L. Wolfrom, The language of particle size, J. GXP Compliance 15 (2011) 10–20.

[21] W.S. Rasband, ImageJ, U.S. National Institutes of Health, Bethesda, Maryland, USA, 1997-2016. http://imagej.nih.gov/ij/.

[22] A. Soldati, L. Baqué, H. Troiani, C. Cotaro, A. Schreiber, A. Caneiro, A. Serquis, High resolution FIB-TEM and FIB-SEM characterization of electrode/electrolyte interfaces in solid oxide fuel cells materials, Int. J. Hydrogen Energy 36

[23] Scribner Associates, ZView for Windows, Version 3.2c, 2010.

[24] L. Baqué, K.P. Padmasree, M.A. Ceniceros Reyes, H. Troiani, M.D. Arce, A. Serquis, A. Soldati, Effect of cobalt-doped electrolyte on the electrochemical performance of LSCFO/CGO interfaces, ECS Trans. 72 (2016) 117–121.

[25] A. Soldati, A. Montenegro-Hernández, L. Baqué, H. Troiani, L. Mogni, A. Schreiber, A. Serquis, Review on ceramic interphases by transmission and scanning electron microscopy, Pract. Metallogr. 51 (2014) 675–688.

[26] A. Montenegro-Hernández, A. Soldati, L. Mogni, H. Troiani, A. Schreiber, F. Soldera, A. Caneiro, Reactivity at the Ln$_2$NiO$_{4+\delta}$/electrolyte interface (Ln = La, Nd) studied by electrochemical impedance spectroscopy and transmission electron microscopy, J. Power Sources 265 (2014) 6–13.

[27] N.J. Simrick, A. Bieberle-Hütter, T.M. Ryll, J.A. Kilner, A. Atkinson, J.L.M. Rupp, An investigation of the oxygen reduction reaction mechanism of La$_{0.6}$Sr$_{0.4}$Co$_{0.2}$Fe$_{0.8}$O$_3$ using patterned thin films, Solid State Ion. 206 (2012) 7–16.

[28] F.S. Baumann, J. Fleig, H.-U. Habermeier, J. Maier, Impedance spectroscopy study on well-defined (La,Sr)(Co,Fe)O$_{3-\delta}$ model electrodes, Solid State Ion. 177 (2006) 1071–1081.

[29] Y.L. Yang, C.L. Chen, S.Y. Chen, C.W. Chu, A. Jacobson, Impedance studies of oxygen exchange on dense thin film electrodes of La$_{0.5}$Sr$_{0.5}$CoO$_{3-\delta}$, J. Electrochem. Soc. 147 (2000) 4001–4007.

[30] S.B. Adler, J.A. Lane, B.C.H. Steele, Electrode kinetics of porous mixed-conducting oxygen electrodes, J. Electrochem. Soc. 143 (1996) 3554–3564.

[31] S.B. Adler, Mechanism and kinetics of oxygen reduction on porous La$_{1-x}$Sr$_x$CoO$_{3-\delta}$ electrodes, Solid State Ion. 111 (1998) 125–134.

[32] S.B. Adler, Factors governing oxygen reduction in solid oxides fuel cell cathodes, Chem. Rev. 104 (2004) 4791–4843.

[33] J. Nielsen, J. Hjelm, Impedance of SOFC electrodes: a review and a comprehensive case study on the impedance of LSM: YSZ cathodes, Electrochimica Acta 115 (2014) 31–45.

[34] J. Nielsen, P. Hjalmarsson, M.H. Hansen, P. Blennow, Effect of low temperature in-situ sintering on the impedance and the performance of intermediate temperature solid oxide fuel cell cathodes, J. Power Sources 245 (2014) 418–428.

[35] L. Baqué, P.S. Jørgensen, W. Zhang, K.V. Hansen, M. Søgaard, Effect of aging on the electrochemical performance of LSM-YSZ cathodes, J. Electrochem. Soc. 162 (2015) F971–F981.

[36] B.A. Boukamp, H.J.M. Bouwmeester, Interpretation of the gerischer impedance in solid state ionics, Solid State Ion. 157 (2003) 29–33.

[37] P. Hjalmarsson, M. Søgaard, M. Mogensen, Oxygen transport properties of dense and porous (La$_{0.8}$Sr$_{0.2}$)$_{0.99}$Co$_{0.8}$Ni$_{0.2}$O$_{3-\delta}$, Solid State Ion. 180 (2009) 1290–1297.

[38] J. Nielsen, T. Jacobsen, M. Wandel, Impedance of porous IT-SOFC LSCF: CGO composite cathodes, Electrochimica Acta 56 (2011) 7963–7974.

[39] E. Bucher, W. Sitte, F. Klauser, E. Bertel, Oxygen exchange kinetics of La$_{0.58}$Sr$_{0.4}$Co$_{0.2}$Fe$_{0.8}$O$_3$ at 600 °C in dry and humid atmospheres, Solid State Ion. 191 (2011) 61–67.

[40] J. Druce, I. Tatsumi, J. Kilner, Surface composition of perovskite-type materials studied by low energy ion scattering (LEIS), Solid State Ion. 262 (2014) 893–896.

[41] M. Kubicek, G.M. Rupp, S. Huber, A. Penn, A.K. Opitz, J. Bernardi, M. Stöger-Pollach, H. Hutter, J. Fleig, Cation diffusion in La$_{0.6}$Sr$_{0.4}$CoO$_{3-\delta}$ below 800 °C and its relevance for Sr segregation, Phys. Chem. Chem. Phys. 16 (2014) 2715–2726.

[42] T. Horita, D.H. Cho, F. Wang, M. Nishi, T. Shimonosono, H. Kishimoto, K. Yamaji, M.E. Brito, H. Yokokawa, Degradation mechanism of SOFC cathodes under CrO$_3$ and SO$_2$ impurity exposures, ECS Trans. 51 (2013) 69–77.